



The Surfactant-Promoted Electroreduction of Oxygen to Hydrogen Peroxide

Reactor Engineering Aspects

Előd L. Gyenge^{*,z} and Colin W. Oloman^{*}

Department of Chemical and Biological Engineering, The University of British Columbia, Vancouver, British Columbia V6T 1Z4, Canada

The two-electron reduction of O₂ at pH 3 (1 M Na₂SO₄ acidified by glacial acetic acid) and 9.6 (mixture of 0.5 M Na₂CO₃ and 0.5 M NaHCO₃) was investigated in flow-by electrochemical reactors with three-dimensional cathodes, consisting of graphite felt (GF) or reticulated vitreous carbon (RVC). The cathode was operated with co-current upward gas/liquid flow and O₂ pressures in the range of 200–700 kPa. A factorial design with four variables at two levels was employed to investigate the effects of superficial current density, liquid load, O₂ pressure, and cationic surfactant concentration [*i.e.*, trioctylmethylammonium chloride (Aliquat® 336, A336)] on H₂O₂ concentration, current efficiency, and reactor voltage. Among the investigated variables A336 exerted the strongest positive main effect on both H₂O₂ concentration and current efficiency. The beneficial effect of A336 was due to suppression of the H₂O₂ loss by both electroreduction and surface-catalyzed decomposition. However, A336 increased the pressure gradient through GF by up to 100%. The surfactant effect on the pressure gradient was estimated using the Herbolzheimer-Park model for the influence of surfactant on the motion of gas bubbles in liquid-filled capillaries. An O₂ mass-transfer model in both GF and RVC was developed and correlated with the experimental results.

© 2005 The Electrochemical Society. [DOI: 10.1149/1.1857773] All rights reserved.

Manuscript submitted March 4, 2004; revised manuscript received August 30, 2004. Available electronically January 28, 2005.

The electrosynthesis of H₂O₂ on an industrial scale is presently practiced only with limited commercial success in spite of a stable peroxide demand growth estimated at 4 to 6% per year in North America, driven mainly by the pulp and paper industry.¹ The only commercial electrochemical technology targeting this market is the on-site alkaline peroxide generation system developed by H-D Tech. (a Dow-Huron joint venture), which is based on the electroreduction of O₂ in a “diaphragm flow control trickle bed” reactor. The electrochemical reactor employs a fixed-bed cathode composed of carbon black and Teflon-coated graphite chips of 40 to 60 mesh.^{2–4} This technology produces typically a 4 wt % H₂O₂ solution in 7 wt % NaOH with a specific energy consumption of 4 kWh kg_{H₂O₂}⁻¹.

A major drawback of the H-D Tech. process is the high alkalinity, 1.7–1.8 NaOH:H₂O₂ weight ratio, of the peroxide product solution. The optimum caustic to peroxide weight ratio for bleaching depends on pulp consistency and type (*e.g.*, chemical, mechanical), bleaching temperature, and retention time. In alkaline peroxide bleaching of chemical pulp the optimum NaOH:H₂O₂ weight ratio is 0.3 for 20–30 wt % pulp consistency and 1.2 in the case of 9–12 wt % consistency, respectively.⁵ Furthermore, recent developments in H₂O₂ pulp bleaching technologies have been aimed at replacing NaOH by Na₂CO₃ as the alkali source. The latter compound imparted superior brightness stability during peroxide bleaching,⁶ gave higher pulp yield, and lowered the chemical oxygen demand (COD) level of the bleaching effluent as compared to NaOH.⁷ Moreover, catalyzed acidic (pH 5) peroxide bleaching technologies have been developed and implemented on an industrial scale.^{8,9}

Unfortunately, the electroreduction of O₂ for large-scale H₂O₂ production at pH < ~13 presently does not meet industrial feasibility requirements such as current efficiency above 80% at current densities of 1–5 kA m⁻², a specific energy less than about 4 kWh kg_{H₂O₂}⁻¹, and a return of investment greater than approximately 30% per year at a H₂O₂ price of about 0.6 \$(US) kg⁻¹. Hydrogen peroxide electrosynthesis at pH < 13 is challenging due mainly to kinetic aspects related to the sluggishness of O₂ electroreduction^{2,10} and the enhanced rate of H₂O₂ electroreduction to H₂O. Regarding the latter, the H₂O₂ reduction current density was found to increase lin-

early with the undissociated H₂O₂ concentration.¹¹ Thus, at pH > pK_{a,H₂O₂} = 11.6 the rate of the secondary reaction decreases markedly with an increase of pH, contributing to a high current efficiency for the 2e⁻ O₂ reduction.

To improve the H₂O₂ formation by O₂ electroreduction in acidic electrolytes various approaches have been explored, such as electrochemical mediation by surface-adsorbed quinone derivatives,^{12,13} electrocatalysis by an electrochemically polymerized Co-tetra(*o*-aminophenol) porphyrin film,¹⁴ and ultrasound-assisted reduction at boron-doped diamond electrodes.¹⁵ None of the above mentioned techniques were evaluated under industrially relevant conditions and reactor designs.

Recently, the present authors have proposed two approaches for O₂ electroreduction to H₂O₂ at pH < 13, the 2-ethyl-9,10-anthraquinone mediated O₂ reduction in a three-phase, aqueous acidic (pH 0.9–3)/organic/gaseous, system^{16,17} and cationic surfactant mediation in a two-phase media, containing an aqueous electrolyte (pH 0.9–11.5) and O₂ gas.¹⁰ The first method, emulsion mediation using an anthraquinone derivative, has been investigated in flow-by three-dimensional electrodes operated with co-current three-phase flow. Using a graphite felt cathode a superficial current density as high as 3000 A m⁻² could be employed with a H₂O₂ current efficiency of 84%.¹⁷ However, the specific energy consumption of the mediated process, was high, *i.e.*, 16–18 kWh kg_{H₂O₂}⁻¹.

Regarding the second method, cationic surfactant mediation in a two-phase (liquid/gas) system, it was found that the presence of a long-chain quaternary ammonium ion *i.e.*, trioctylmethylammonium chloride [CH₃(C₈H₁₇)₃N⁺Cl⁻, trade name Aliquat® 336 abbreviated as A336] in the aqueous electrolyte, increased the standard heterogeneous rate constant for the 2e⁻ O₂ reduction on glassy carbon in the pH range 0.9 (*i.e.*, 0.1 M H₂SO₄) to 11.5 (*i.e.*, 0.1 M Na₂CO₃).¹⁰ This effect has been attributed to an increase of the cathode surface pH in the presence of adsorbed quaternary ammonium ions. Moreover, batch electrolysis using reticulated vitreous carbon (RVC) cathodes showed that the presence of A336 at millimol (mM) levels improved certain figures of merit for H₂O₂ electrosynthesis, such as the accumulated H₂O₂ concentration and the current efficiency for H₂O₂ generation.¹⁰

Therefore, it was of interest to investigate the effect of A336 on the two-phase O₂ reduction under conditions closer to potential industrial applications, employing continuous flow reactors. Due to

* Electrochemical Society Active Member.

^z E-mail: egyenge@chml.ubc.ca

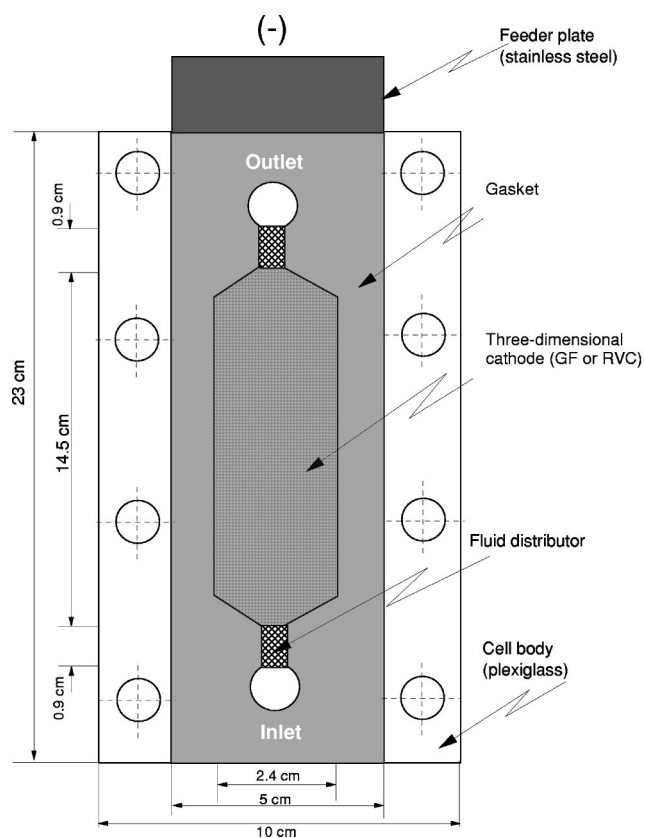


Figure 1. Front view of the cathode compartment.

the multivariable nature of the process, a statistical experimental design approach has also been employed. This is the first investigation looking at the effect of a cationic surfactant on the reactor engineering of O_2 electroreduction in flow-by fiber-bed and reticulated electrodes.

In addition to pulp bleaching, the potential applications of an efficient H_2O_2 electrosynthesis method at $pH < 13$ are numerous, including the paired electrosynthesis of benzaldehyde from toluene mediated by H_2O_2 and the V^{5+}/V^{4+} redox couple¹⁸ or degradation of organic effluents, such as formaldehyde,^{19,20} phenol, cresol, catechol, *p*-benzoquinone, anilin, oxalic acid, and dyes by H_2O_2 .^{21,22}

Experimental

Figure 1 shows a front view of the cathode compartment in the flow-by electrochemical reactor equipped with either a graphite fiber bed (GF, referred to also as graphite felt) or reticulated vitreous carbon (RVC, ~ 39 ppc (pores per centimeter), *i.e.*, 100 ppi (pores per inch)]. Table I and Fig. 2 show certain physicochemical and structural characteristics for GF (The Carborundum Co., Sanborn, NY) and RVC (ERG Materials & Aerospace Co., Oakland, CA). The

Table I. Physicochemical characteristics of the three-dimensional electrodes.

Property	GF (compressed by 38%)	RVC	Reference/ source
Specific surface area, $m^2 m^{-3}$	16,000	6,560	17
Electronic conductivity, $S m^{-1}$	23	62	17
Porosity	0.92	0.95	17
Mean fiber diameter, $\times 10^{-6}$ m	20	53	Fig. 2

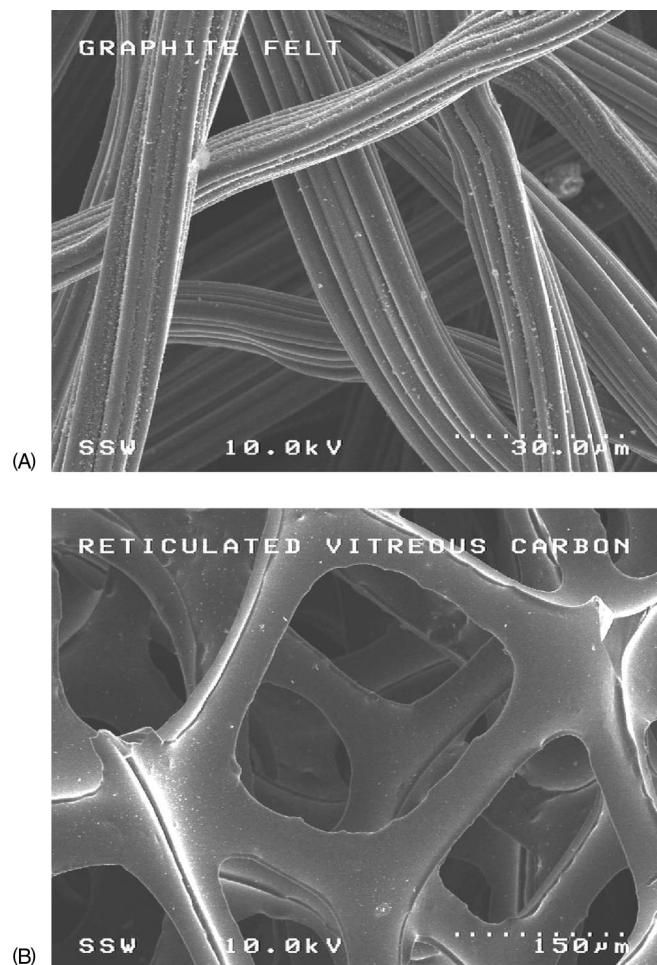


Figure 2. SEM images of: (A) GF and (B) RVC.

specific electronic conductivity of the RVC was 2.7 times higher than for GF, while the latter had a higher specific surface area, *i.e.*, $16,000 m^2 m^{-3}$ vs. $6,560 m^2 m^{-3}$ RVC. Figure 2 reveals the open-cell (foam-like) structure of RVC as compared to the irregular arrangement of fibers in GF. In addition to structural difference, energy dispersive X-ray analysis (EDX), X-ray photoelectron spectroscopy (XPS), and Fourier transform infrared spectroscopy (FTIR) analysis indicated surface composition differences between the two types of carbons.

The surface of GF had virtually no oxidized carbon, being composed entirely of graphitic carbon. On the other hand the surface of RVC showed oxidized carbon in the form of hydroxyl, ester, and carbonyl functional groups. The oxygen content of RVC surface was determined by XPS analysis as about 8 atom %. Furthermore, FTIR analysis revealed that GF is composed of graphitic carbon only, while RVC shows C-H and C-C bonds that are characteristic for hydrocarbons. The differences in surface-functional groups could impact the electrocatalytic properties of the carbon electrodes under investigation.

The cathode thickness in the reactor (Fig. 1) was 4.5×10^{-3} m, corresponding in the case of GF to 38% compression (uncompressed thickness 7.25×10^{-3} m). The superficial cathode area in the direction of current flow was $33 \times 10^{-4} m^2$, while the area in the direction of fluid flow was $1.1 \times 10^{-4} m^2$. The cathode was operated in flow-by arrangement (the current and fluid flow directions perpendicular on each other) with co-current upward O_2 gas-liquid flow. The two-phase pressure drop along the cathode height was measured with Bourdon gauges connected at the inlet and outlet ports of the cathode compartment.

The GF three-dimensional electrode was placed on a stainless steel current feeder plate and fitted into Durabla® gaskets (Fig. 1). The reactor with the GF cathode was uniformly compressed using a torque wrench set to 5 foot-pound. In the case of the reticulated vitreous carbon cathode, a graphite fiber paper of 3×10^{-4} m thickness was inserted between the stainless steel current feeder plate and RVC to assure good electric contact. The reactor with the RVC fixed-bed embedded tightly into gaskets was carefully sealed to avoid compression and crushing of the rigid reticulated structure. The anode for alkaline conditions was Ni felt (7×10^{-4} m thick), while for acidic conditions a dimensionally stable O₂ anode (DSA) plate was employed.

The reactor body was made of Plexiglas plates. The entrance and exit regions of the cathode contained a plastic mesh acting as a fluid distributor. The cathode and anode compartments were separated by a cation exchange membrane (Nafion 350) supported on the anode side by a plastic mesh. The anolyte was either 1.5 M NaOH or 0.5 M Na₂SO₄ at pH 3, both in upward flow. The catholyte was either a mixture of 0.5 M Na₂CO₃-0.5 M NaHCO₃ at pH 9.6 (at 293 K) or 1 M Na₂SO₄ acidified to pH 3 (at 293 K) with glacial acetic acid. The absolute O₂ pressure in the cathode compartment was varied between 200 and 700 kPa. The arrangement of reactor components and the external flow circuit have been described previously.¹⁷ The average temperature in the reactor during electrosynthesis was 300 ± 7 K. After about half-an hour run at each set of operating conditions with single-pass catholyte, the outlet catholyte stream was sampled and analyzed for H₂O₂ content by redox titration with KMnO₄ in H₂SO₄ 20 wt %.²³ In the present work no peroxide stabilization agent was added to the catholyte.

The effect of a triple C₈-chain quaternary ammonium salt, CH₃(C₈H₁₇)₃N⁺Cl⁻ (triethylmethylammonium chloride, trade name Aliquat 336, abbreviated as A336, Sigma-Aldrich, Inc.) dispersed in the catholyte at concentrations up to 3 mM was investigated by both parametric and factorial experiments. The factorial experimental design and analysis was executed using the Jass 2.1 software (Joiner Associates, Madison, WI).

Furthermore, the effect of surfactants on the electroreduction of H₂O₂ at 298 K was studied in separate-batch electrolysis experiments using a stirred H-cell equipped with an RVC cathode of 1×10^{-3} m² effective superficial area. Coulometry experiments were performed in deoxygenated (N₂ purge) 0.1 M Na₂CO₃ and H₂SO₄ solutions containing initially *ca.* 1 M H₂O₂ (prepared from 30 wt % stock solution, Fisher Scientific, Inc.). The peroxide solution contained no stabilizing agent. The cathode superficial current density was kept constant at 300 A m⁻² and the residual H₂O₂ concentration after 15 min of electrolysis was determined. In addition to A336, a nonionic and an anionic surfactant were also tested for potential effect on H₂O₂ electroreduction, *i.e.*, Triton X-100 [C₁₄H₂₂O(C₂H₄O)_{*n*}, with *n* = 9-10, Sigma-Aldrich, Inc.] and sodium dodecylsulfate (SDS, C₁₂H₂₅OSO₃⁻Na⁺, Sigma-Aldrich, Inc.).

Results and Discussion

The effect of cationic surfactant (A336) on the electroreduction of H₂O₂.—Complementary to the influence of A336 on the 2e⁻ O₂ electroreduction,¹⁰ in the context of H₂O₂ electrosynthesis it was of interest to evaluate the effect of the quaternary ammonium ion on the secondary reaction of H₂O₂ electroreduction. The thermodynamics of O₂ and H₂O₂ electroreduction are (*E*^o values at pH 0 and 14, respectively, from Ref. 11)

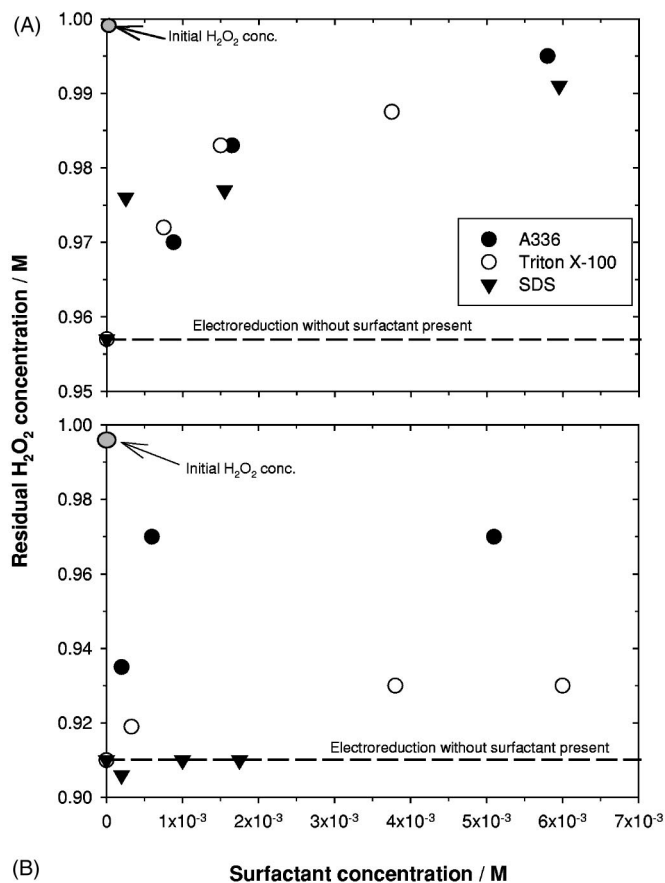
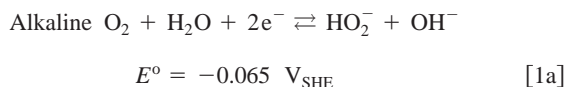


Figure 3. Influence of surfactants on the galvanostatic electroreduction of H₂O₂ on RVC 12 ppc cathode. Current density: 300 A m⁻², time 15 min, 298 K, N₂ purge. Electrolyte: (A) 0.1 M H₂SO₄, (B) 0.1 M Na₂CO₃. Legend: (●) A336, (○) Triton X-100, (▼) SDS.



Afanas'ev *et al.* reported the inhibiting effect of certain quaternary ammonium salts on H₂O₂ electroreduction in NaCl 3.16 wt % on a dropping Hg electrode. These authors found that the inhibiting effect increased with hydrocarbon chain length, *e.g.*, (C₄H₉)₄N⁺ ion was more effective than the (CH₃)₄N⁺ ion.²⁴ In the present work the comparative influence on peroxide electroreduction on RVC of A336 and representative nonionic and anionic surfactants, *i.e.*, Triton X-100 and SDS, respectively, has been assessed using a stirred H cell. The residual peroxide concentration after 15 min of galvanostatic operation at 300 A m⁻² is shown in Fig. 3. The initial peroxide concentration was close to 1 M.

In the absence of additives the residual peroxide concentrations were 0.91 M in 0.1 M Na₂CO₃ and 0.96 M in 0.1 M H₂SO₄, *i.e.*, 8.5 and 4.3% peroxide loss in 15 min, respectively. These values reflect H₂O₂ losses by three possible mechanisms, intrinsic electroreduction (Eq. 1b and 2b) and two non-faradaic mechanisms, *i.e.*, heterogeneous, surface-catalyzed, decomposition (*i.e.*, effect of electrode material and possibly reaction vessel materials) and homogeneously catalyzed, bulk decomposition, which is pH and electrolyte composition dependent. Decomposition in the bulk is promoted by an increase of pH, the presence of transition metal ions [*e.g.*, Fe(II), Mn(II), Cu(II)] and carbonate ions.²⁵

It is difficult to differentiate among the three potential peroxide loss mechanisms since synergistic effects are likely to occur, *e.g.*, during electroreduction (Eq. 1 and 2) the surface pH increases which in turn raises the rate of non-faradaic H₂O₂ decomposition. In separate experiments without current but with the RVC in the cathode

chamber, it was found that the non-faradaic decomposition in acid accounted for about 1% loss of H_2O_2 in 15 min (residual concentration of 0.99 M), while in carbonate the corresponding loss was about 5.5% during the same time interval (*i.e.*, residual peroxide concentration about 0.94 M). Thus, it can be concluded that with current (*i.e.*, at 300 A m^{-2}), electroreduction contributed about 3.3 and 3%, respectively, to the total peroxide loss in 0.1 M H_2SO_4 and 0.1 M Na_2CO_3 . The latter values are slightly above (by about 1%) those expected from Faraday's law assuming 100% current efficiency. This result indicates possible interaction effects (such as an increase of surface pH) contributing to peroxide loss by a non-faradaic route.

It is proposed, therefore, that in acid the electroreduction of peroxide is the main pathway for H_2O_2 loss, while in carbonate both electroreduction and non-faradaic routes contribute to peroxide loss, with the latter mechanism being more significant at 300 A m^{-2} . These findings are corroborated by the study of Kolyagin and Kornienko who investigated the H_2O_2 decomposition rates in acidic and alkaline solutions on gas-diffusion electrodes prepared with hydrophobized carbon black and operated at 500 A m^{-2} .²⁶ However, considering that the rate of electroreduction is potential-dependent it is expected that the relative contribution of the electrochemical pathway to the total peroxide loss will increase with current density.

In 0.1 M H_2SO_4 (Fig. 3A) all three surfactants, cationic: A336, non-ionic: Triton X-100 and anionic: SDS, reduced the loss of H_2O_2 . Surfactant concentrations above 3 mM reduced the H_2O_2 loss to levels corresponding approximately to non-faradaic decomposition only. In 0.1 M Na_2CO_3 , on the other hand (Fig. 3B), the anionic surfactant SDS was ineffective (*i.e.*, the residual H_2O_2 concentration was the same as in the absence of surfactant). However, both A336 and Triton X-100 suppressed the H_2O_2 loss, while A336 was more effective. Furthermore, A336 was the only additive, which suppressed both the faradaic and the surface-catalyzed non-faradaic peroxide loss (Fig. 3B).

Figure 4 shows the cathode potentials at 300 A m^{-2} for H_2O_2 reduction in the presence and absence of surfactants after 1 min of electrolysis. In acid, millimole levels of all three surfactants decreased the H_2O_2 cathode reduction potential. The potential shifted from $-1.05 \text{ V vs. Ag/AgCl, KCl}_{\text{std}}$ without surfactant to about -2.2 and -2.4 V with surfactant present (Fig. 4A). In carbonate, A336 brought about the largest decrease of cathode potential, *i.e.*, from -0.9 to about -1.7 V , while SDS left the H_2O_2 reduction potential unchanged at around -0.9 V (Fig. 4B). These data suggest clearly that the effectiveness of surfactants in repressing the H_2O_2 loss is related to changes occurring on the electrode surface, induced most likely by surfactant adsorption (both electrostatic and specific). In alkaline media the electrosorption of both SDS (anionic) and Triton X-100 (non-ionic) is less favored as compared to the cationic surfactant A336. Thus, the former are not effective suppressors of H_2O_2 electroreduction. In acid (pH 0.9) on the other hand, both SDS and Triton X-100 undergo protonation, canceling out to some extent the electrostatic repulsion encountered at the cathode surface. Thereby, they are almost as effective as A336 in lowering the H_2O_2 electroreduction rate.

In addition to the inhibiting effect of A336 on H_2O_2 electroreduction investigated here, it has been previously found, as indicated in the introduction, that A336 improved the two-electron O_2 reduction kinetics.¹⁰ Therefore, the cationic surfactant, trioctylmethylammonium chloride (A336), has been retained as an additive for O_2 electroreduction to H_2O_2 in flow-by reactors.

Comparative investigation of graphite felt and reticulated vitreous carbon cathodes in flow-by reactors.—Graphite felt and reticulated vitreous carbon 39 ppc were tested as cathodes for O_2 reduction in both alkaline (pH 9.6) and acidic (pH 3) solutions, in the presence and absence of the cationic surfactant A336 (Experimental section). The flow-by reactor was operated with co-current upward gas/liquid flow, O_2 gas load of $0.16 \text{ kg m}^{-2} \text{ s}^{-1}$, and liquid

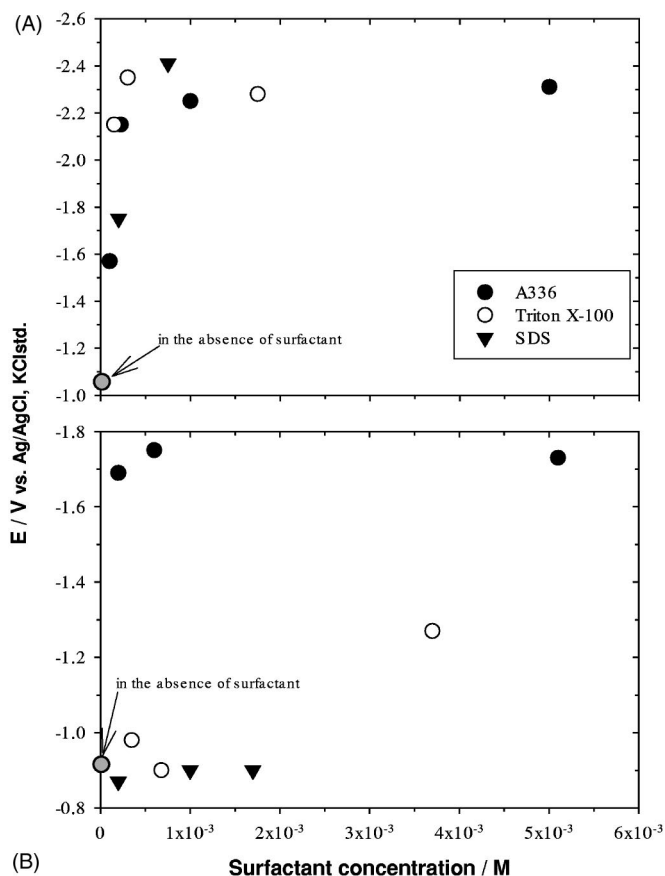


Figure 4. Cathode potentials measured after 1 min of H_2O_2 electroreduction under galvanostatic operation at 300 A m^{-2} . Cathode: RVC 12 ppc. Conditions identical to Fig. 3. Electrolyte: (A) 0.1 M H_2SO_4 , (B) 0.1 M Na_2CO_3 . Legend: (●) A336, (○) Triton X-100, (▼) SDS.

load of $4.5 \text{ kg m}^{-2} \text{ s}^{-1}$. The liquid-to-gas load ratio ensured a surging flow regime.²⁷ The absolute outlet pressure was 350 kPa for alkaline and 425 kPa for acidic conditions, respectively.

Comparing Fig. 5 and 6 reveals that in the alkaline solution (pH 9.6), regardless of the surfactant presence, the peroxide concentrations generated per single pass are higher for GF than for RVC at superficial current densities above 500 A m^{-2} . The GF cathode, could be operated at current densities as high as 4000 A m^{-2} with a current efficiency close to 70% with 3 mM A336 in the electrolyte (Fig. 5, inset). In the case of RVC in the presence of A336, a current efficiency of about 70% was obtained at a superficial current density of only 700 A m^{-2} .

The difference in performance between RVC and GF at superficial current densities above about 500 A m^{-2} can be explained by a mass-transfer model that estimates the superficial mass-transfer limiting current density for O_2 reduction and the corresponding maximum electroactive bed thickness (Appendix A).

In the case of the alkaline electrolyte, for the employed liquid and gas loads, the mass-transfer limiting superficial current densities in the absence of surfactant were about 370 A m^{-2} for RVC and 1520 A m^{-2} for GF, respectively (Appendix A, Table A-I). Figure 5 and 6 show for both three-dimensional electrodes at superficial current densities below the respective mass-transfer limiting values, oxygen was reduced to H_2O_2 , with current efficiencies above 75% regardless of A336 presence. The corresponding maximum electroactive thickness was only 0.6 mm for GF and 2.5 mm for RVC, compared to the geometric bed thickness of 4.5 mm. Thus, due to the nonlinear potential and current distribution across the three-dimensional electrode only a fraction of the bed thickness is capable

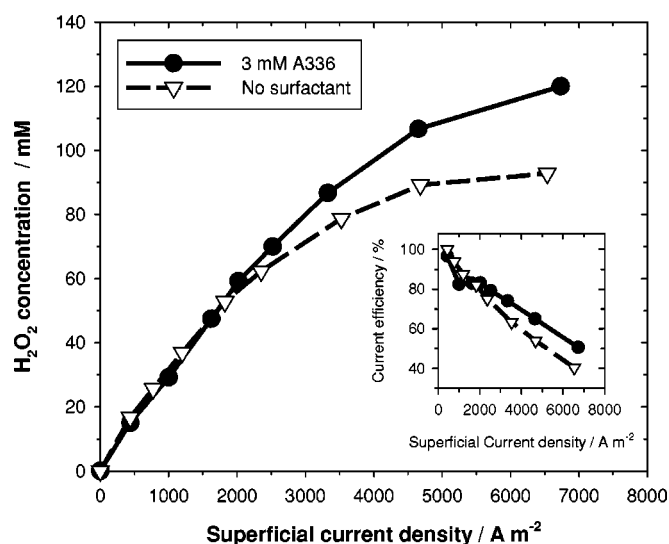


Figure 5. Electroreduction of O_2 in $0.5\text{ M Na}_2\text{CO}_3$ - 0.5 M NaHCO_3 (pH 9.6) in a flow-by reactor with GF cathode operated with two-phase upward G/L flow. Temperature: 300 K, liquid load: $4.5\text{ kg m}^{-2}\text{ s}^{-1}$. Gas load: $0.16\text{ kg m}^{-2}\text{ s}^{-1}$, pressure 350 kPa. Legend: (●) 3 mM A336 and (▽) without surfactant. Inset: current efficiency for H_2O_2 .

of working at the limiting current density without significant side reactions.

The calculated limiting current density for RVC (*i.e.*, 370 A m^{-2}) is corroborated by the experimental data of Davison *et al.* that showed current efficiencies for H_2O_2 generation on RVC above 80% only for superficial current densities below 500 A m^{-2} (O_2 reduction in 2 M NaOH at 1725 kPa absolute pressure).²⁸

The presence of A336 influences the polarization curve of O_2 reduction¹⁰ and the overpotential of H_2O_2 electroreduction (Fig. 4). Thus, A336 will affect the maximum allowable potential drop $\Delta\Phi_{\text{max},I}$ that can be tolerated without significant secondary reaction in the three-dimensional electrode. Consequently, A336 will have an effect on both the maximum electroactive bed thickness and the

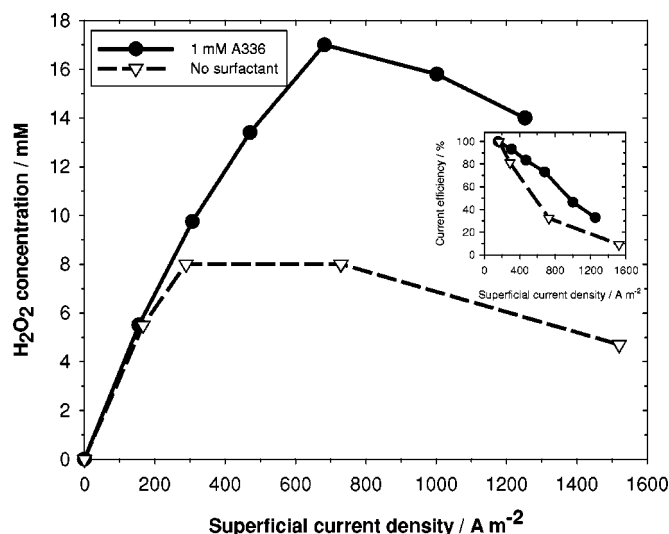


Figure 6. Electroreduction of O_2 in $0.5\text{ M Na}_2\text{CO}_3$ - 0.5 M NaHCO_3 (pH 9.6) in a flow-by reactor with RVC 39 ppc cathode and two-phase upward G/L flow. Temperature: 300 K, liquid load: $4.5\text{ kg m}^{-2}\text{ s}^{-1}$. Gas load: $0.16\text{ kg m}^{-2}\text{ s}^{-1}$, pressure: 350 kPa. Legend: (●) 1 mM A336 and (▽) without surfactant. Inset: current efficiency for H_2O_2 .

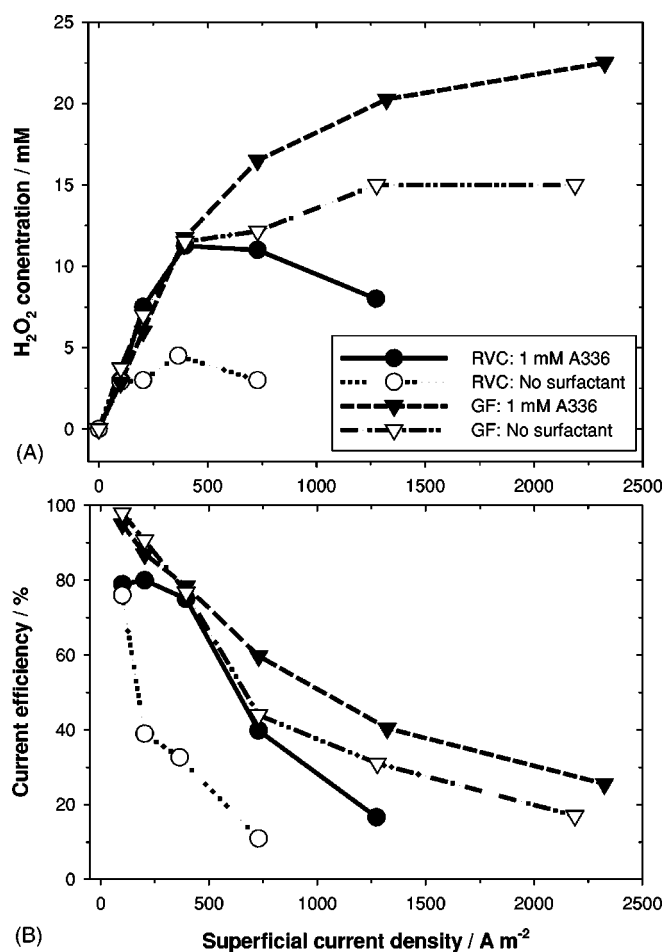


Figure 7. Electroreduction of O_2 in $1\text{ M Na}_2\text{SO}_4$ (pH 3 acidified with glacial acetic acid). Comparison between GF and RVC 39 ppc cathodes. Flow-by reactor with two-phase upward G/L flow. Temperature: 300 K, liquid load: $4.5\text{ kg m}^{-2}\text{ s}^{-1}$. Gas load: $0.16\text{ kg m}^{-2}\text{ s}^{-1}$, pressure: 425 kPa. (A) H_2O_2 concentration per pass; (B) current efficiency. Legend: (●) RVC, 1 mM A336, (○) RVC, without surfactant, (▼) GF, 1 mM A336, (▽) GF, without surfactant.

superficial limiting current density for O_2 reduction, as shown in Appendix A. With surfactant present, it is estimated that the maximum electroactive thickness increased to 0.9 mm for GF and 4.1 mm for RVC (*i.e.*, almost equal to the geometric thickness of RVC) (Table A-I, Appendix A). The corresponding superficial limiting current densities were higher, therefore, than without A336 present, *i.e.*, 2760 and 680 A m^{-2} for GF and RVC, respectively.

For GF (Fig. 5) the current efficiency corresponding to the O_2 mass-transfer limited superficial current density was about 75%. At current densities higher than 2760 A m^{-2} the H_2O_2 accumulation rate diminished and the current efficiency dropped below 75%.

Correlating the O_2 mass-transfer limited superficial current density with the experimental results in the case of RVC (Fig. 6), it is observed that with surfactant the H_2O_2 concentration increased with current density up to the mass-transfer limited value of 680 A m^{-2} where the current efficiency was close to 70%. At current densities above 680 A m^{-2} both the H_2O_2 concentration and current efficiency dropped, as expected, due to the increased significance of the secondary reaction (*i.e.*, H_2O_2 electroreduction).

In the case of the acidic solution on the other hand (Fig. 7), using either GF or RVC cathode current efficiencies for H_2O_2 generation of and above 75% were obtained only at superficial current densities below 500 A m^{-2} . This observation is consistent with the electrode kinetic limitation of O_2 reduction in acidic media. The presence of 1

Table II. Variables and their levels for the 2⁴ + 1 factorial runs in 0.5 M Na₂CO₃-0.5 M NaHCO₃ (pH 9.6). Cathode: GF, temperature: 300 K, O₂ gas load: 0.27 kg m⁻² s⁻¹.

No.	Variables (Symbols, units)	Levels		
		Low (-)	Center (0)	High (+)
1	Current density; <i>i</i> (A m ⁻²)	927	2780	4650
2	Catholyte load; <i>L</i> (kg m ⁻² s ⁻¹)	1.7	5.3	7.8
3	Pressure; <i>P</i> ^a (kPa)	200	350	475
4	A336 conc.; <i>S</i> (mM)	0	1	3

^a Absolute outlet reactor pressure.

mM A336 was beneficial for H₂O₂ electrosynthesis using both electrodes. In the case of GF operated at 750 A m⁻², the surfactant raised the current efficiency from 42 to 60%. Using RVC at 300 A m⁻² in the absence of surfactant the current efficiency was only about 30%, while with 1 mM A336 the H₂O₂ current efficiency improved to 75% (Fig. 7).

The calculated limiting superficial current densities and the maximum electroactive bed thickness were lower at pH 3 compared to pH 9.6 (Table A-I, Appendix A), due to the decrease of ΔΦ_{max,I} (Appendix A) as a consequence of the enhanced rate of H₂O₂ reduction in acid.¹¹ The cationic surfactant had a positive effect on both H₂O₂ concentration and current efficiency (Fig. 7). In the case of RVC, A336 increased the limiting superficial current density from 260 A m⁻² (without) to 470 A m⁻² (with A336) (Appendix A). Consequently, for the latter current density value (Fig. 7), the H₂O₂ current efficiency was about 70% with A336 and only 27% in its absence.

To evaluate and quantify the main and synergistic effects of four process variables, superficial current density, liquid-to-gas load ratio, pressure, and A336 concentration, factorial experiments were carried out. Graphite felt was retained as the cathode of choice.

Alkaline electrolyte pH 9.6: factorial experiments.—With a catholyte composed of 0.5 M Na₂CO₃ and 0.5 M NaHCO₃ factorial experiments were performed using four variables at two levels and one centerpoint (*i.e.*, 2⁴ + 1 design, Table II). The superficial current densities used in the factorial design were chosen such that the low value of 927 A m⁻² is below while the high value of 4650 A m⁻² is above the mass-limiting superficial current density for O₂ reduction under the conditions employed in the factorial design. The liquid flow rates were 1.67 × 10⁻⁷ m³ s⁻¹ and 7.5 × 10⁻⁷ m³ s⁻¹ at the low and high load level (Table II), respectively. The corresponding calculated average residence times in the cathode compartment were 20 and 90 s. The gas load was constant 0.27 kg m⁻² s⁻¹. Increasing the liquid load from low to high changed the flow regime from pulsing to surging flow.²⁷ The outlet absolute pressure ranged between 200 and 475 kPa.

Table III shows the complete set of the seventeen factorial runs, as designed with the aid of the Jass 2.1 software, and the figures of merit (*i.e.*, H₂O₂ concentration, current efficiency, and reactor voltage). The outlet pH varied between 9.7 (for high flow rate coupled with low current density) and 12.5 (low flow rate-high current density combination). The operating temperature was 300 ± 7 K.

Table III shows that H₂O₂ concentrations higher than 300 mM could be obtained with current efficiencies above 60% for combinations of low liquid load and high current density levels (*e.g.*, runs no. 5, 7, 9, and 17, in Table III).

Based on the factorial experimental design results the main and interaction effects were calculated with the Jass 2.1 software. Furthermore, using the main and interaction effects the factorial re-

Table III. Design matrix and responses (in random order) for the factorial runs in 0.5 M Na₂CO₃-0.5 M NaHCO₃ (pH 9.6).

No.	Variable levels				H ₂ O ₂ concentration ^a (mM)	Current efficiency ^b (%)	Reactor voltage ^c (V)
	<i>i</i>	<i>L</i>	<i>P</i>	<i>S</i>			
1	-	-	+	+	78	82	2.85
2	+	+	-	+	62	59	6.30
3	-	+	-	-	18	85	2.60
4	-	-	-	-	80	85	2.55
5	+	-	-	-	301 ± 13	63 ± 3	5.50 ± 0.07
6	+	+	+	-	72	68	5.60
7	+	-	-	+	400 ± 9	84 ± 2	5.22 ± 0.24
8	0	0	0	0	77 ± 2	83 ± 2	4.50
9	+	-	+	+	350 ± 7	74 ± 3	5.50 ± 0.33
10	-	+	-	+	20.5	97	2.85
11	-	-	-	+	83	88	2.60
12	+	+	-	-	50 ± 2	47 ± 2	5.80
13	+	+	+	+	81	77	5.70
14	-	-	+	-	78	82	2.50
15	-	+	+	+	21	100	2.50
16	-	+	+	-	20	95	2.45
17	+	-	+	-	364 ± 5	77 ± 1	5.20

^a Average response: 128 mM. Pooled standard deviation: ±8.3 mM.

^b Average response: 79%. Pooled standard deviation: ±2.4%.

^c Average response: 4.13 V. Pooled standard deviation: ±0.24 V.

sponses can be expressed as a regression model.²⁹ The three figures of merit considered here, *i.e.*, H₂O₂ concentration *C*_{H₂O₂} (mM), current efficiency CE (%), and reactor voltage, *E*_{reactor} (V), could be described by the following regression equations (statistically insignificant effects were neglected)

$$C_{H_2O_2}(\text{mM}) = 128 + 80.1X_I - 87.2X_L + 7.7X_S - 56.9X_I X_L + 6.2X_I X_S - 7.45X_P X_S - 6.95X_I X_P X_S + 7X_L X_P X_S \quad [3]$$

$$CE(\%) = 79 - 10.3X_I + 2.95X_P + 3.6X_S - 5.45X_I X_L + 2.45X_I X_P + 3.55X_L X_P - 2.3X_P X_S \quad [4]$$

$$E_{\text{reactor}}(\text{V}) = 4.13 + 1.49X_I, \quad [5]$$

where the coded variables are defined as $X_I = (i - 2788.5)/1861.5$, $X_P = (P - 337.5)/137.5$, $X_S = (S - 1.5)/1.5$, and $X_L = (L - 4.75)/3.05$, with *i* the superficial current density (A m⁻²), *L* liquid load (kg m⁻² s⁻¹), *P* absolute pressure (kPa), and *S* the A336 concentration (mM).

Equation 3-5 show that in the factorial experiments the average H₂O₂ concentration per pass and current efficiency were 128 ± 8.3 mM and 79 ± 2.4%, respectively, associated with an average reactor voltage of 4.13 ± 0.24 V. The regression equations for H₂O₂ concentration and current efficiency can be represented as contour plots. Figure 8 depicts the interaction between the superficial current density (*i.e.*, given as coded variable *X*_I) and liquid load (*i.e.*, *X*_L) corresponding to *X*_S = 1 and *X*_P = -1 (*i.e.*, high concentration of A336 and low pressure). For the employed reactor design the contour plot shows (Fig. 8) that a H₂O₂ concentration per pass of 350 mM (or higher) is achievable with a current efficiency of 75-80% as long as *X*_I is in the range of 0.8 to 1.0 while *X*_L is between -0.8 and -1.0. The corresponding reactor voltage is expected to be in the range of 5.3-5.6 V. On the other hand, current efficiencies greater than 90% can only be obtained for *X*_I ≤ -0.6. Under the latter condition, the expected H₂O₂ concentration per pass is ≤150 mM depending on *X*_L. Thus, there is an obvious trade-off between current efficiency and H₂O₂ concentration.

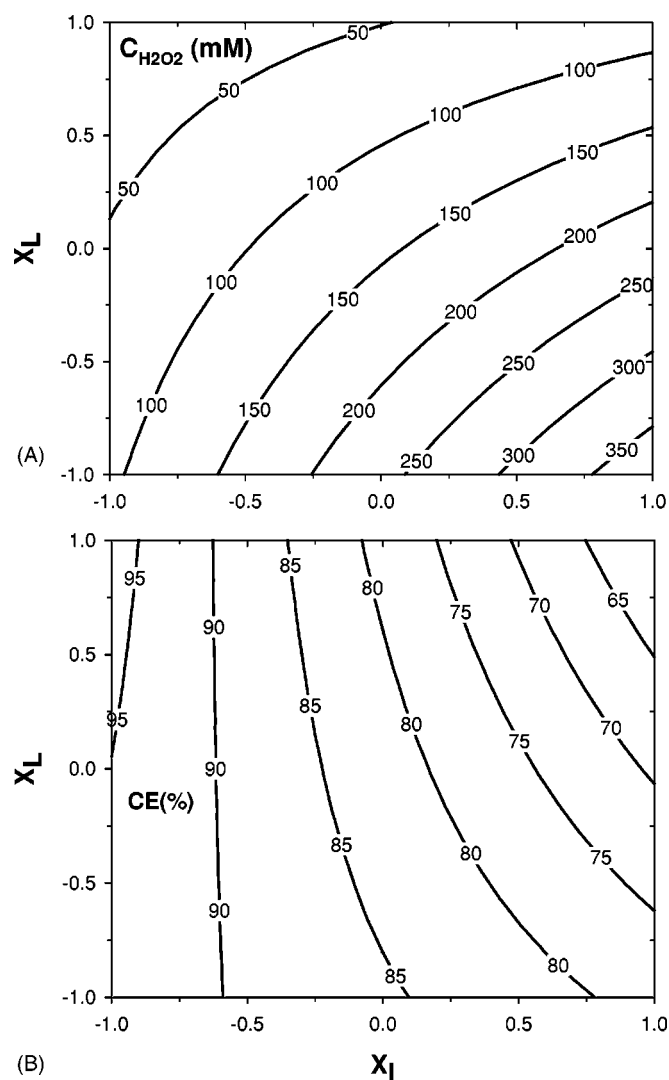


Figure 8. Contour plot of the factorial regression model for electroreduction of O₂ in 0.5 M Na₂CO₃-0.5 M NaHCO₃ (pH 9.6) on GF. $X_S = 1$ and $X_P = -1$. (A) H₂O₂ concentration, (B) current efficiency.

As shown by Eq. 4, with respect to current efficiency the surfactant concentration had the second most significant effect after current density. Interestingly, the surfactant main effect was higher than the main effect of pressure, as indicated by the respective coefficients in the regression Eq. 4. At a high level of current density, low liquid load and pressure, with 3 mM A336 present in the electrolyte the peroxide concentration increased by about 33%, *i.e.*, from 300 to 400 mM (compare runs no. 5 and 7, Table III, current efficiency of 63 and 84%, respectively).

Furthermore, the surfactant and pressure had a negative two-factor interaction and the three-factor interaction including the superficial current density was negative as well (Eq. 3 and 4). In other

words, increasing the operating pressure from low to high when A336 is at the high (*i.e.*, 3 mM) level was not beneficial (especially in the case of high current density level, *e.g.*, compare runs no. 7 and 9, Table III).

To explain the pressure-surfactant interaction, one has to consider the flow conditions in the graphite felt electrode in the presence of surfactant. At high pressure (475 kPa) the radii of the O₂ bubbles decreases, therefore, the specific gas-liquid (G/L) interfacial area increases under the same conditions. For trickle-bed reactors it was found that the specific G/L interfacial area increased with gas pressure for superficial gas velocities exceeding 0.02-0.03 m s⁻¹ (for a review see Ref. 30). For the present case the superficial O₂ velocity was 0.2 m s⁻¹ at STP (or 0.045 m s⁻¹ at 475 kPa, 307 K), therefore, it is likely that the G/L interfacial area increased with pressure from low (200 kPa) to high (475 kPa). A sample calculation is presented at the end of the present section.

The increase of the G/L interfacial area causes a local decrease of surfactant excess concentration at the G/L interface, hence, a local increase of surface tension. In order to counteract the local increase of surface tension, mass transfer of surfactant occurs from the bulk liquid to the G/L interface.^{31,32} The surfactant mass transfer to the G/L interface could decrease the surfactant concentration at the solid-liquid interface. Consequently, the ability of A336 to adsorb and form surface structures on the electrode that are effective in suppressing H₂O₂ electroreduction and/or decomposition, is diminished. It is hypothesized, therefore, that the negative interaction between surfactant and pressure is related to G/L surface tension gradients generated at high operating pressures (*e.g.*, 475 kPa).

One way to test experimentally the discussed hypothesis based on surface tension gradients is to compare the pressure drop through the graphite felt with and without the presence of A336. There is experimental evidence indicating that the pressure drop associated with the movement of gas bubbles in liquid-filled capillaries, increases in the presence of surfactants.³¹ A 50 to 100 times higher two-phase pressure drop was reported for co-current upward G/L flow through graphite felt in the presence of the foaming agent Tergitol (at 0.1% volume ratio of surfactant to liquid).³³ The theoretical explanation put forward by Herbolzheimer (1988, quoted by Probst, ^{31a}) and Park (1992, ^{31b}), relies on the fact that the pressure drop increase with surfactant is due to an increase of the Laplace pressure difference between the front and rear of the gas bubble as a result of surfactant accumulation at the rear. In other words, a surface tension difference develops between the front and rear menisci of the bubble, with $\Delta\gamma = \gamma_{\text{front}} - \gamma_{\text{rear}} > 0$. Thus, the drag force acting on the bubble in the rigid liquid film region increases in the presence of surfactant.³¹

In the present work the two-phase liquid-gas (L/G) pressure gradient has been measured with and without 3 mM A336 in the electrolyte, *i.e.*, $\Delta p_{LG,A336}$ and Δp_{LG} , respectively. Table IV shows the two pressure gradients as a function of liquid load at an operating pressure of 475 kPa. The measured two-phase pressure gradient in the absence of surfactant Δp_{LG} , at a liquid load of 1.7 kg m⁻² s⁻¹ matched fairly well (standard deviation about 10%) the value predicted for fiber beds by the Hodgson and Oloman correlation.³⁴

At 475 kPa(abs) operating pressure the presence of 3 mM A336 increased the two-phase pressure gradient by 70 to 100% (Table IV). For a liquid load of 1.7 kg m⁻² s⁻¹ the pressure gradient doubled

Table IV. The effect of surfactant concentration (A336) on the pressure gradient in the graphite fiber bed with co-current upward two-phase (gas-liquid) flow. Gas (O₂) load 0.27 kg m⁻² s⁻¹, pressure 475 kPa (abs). For calculations see Appendix B.

Liquid load L (kg m ⁻² s ⁻¹)	$\Delta p_L \times 10^5$ (Pa m ⁻¹)	Without surfactant			A336 concentration = 3 mM		
		$\Delta p_{LG} \times 10^5$ (Pa m ⁻¹)	$\Delta p_G \times 10^5$ (Pa m ⁻¹)	$\Delta p_{G,\gamma}^* \times 10^5$ (Pa m ⁻¹)	$\Delta p_{LG,A336} \times 10^5$ (Pa m ⁻¹)	$\Delta p_{G,A336} \times 10^5$ (Pa m ⁻¹)	$\Delta p_{G,\gamma}^* \times 10^5$ (Pa m ⁻¹)
1.7	0.11	1.72	0.29	0.27	3.45	0.88	0.88
7.8	0.49	3.45	0.21	0.21	5.86	0.77	0.78

Table V. Variables and their levels for the $2^4 + 1$ factorial runs in 1 M Na_2SO_4 (pH 3 acidified with glacial acetic acid). Cathode: GF, temperature: 300 K and O_2 gas load $0.47 \text{ kg m}^{-2} \text{ s}^{-1}$.

No.	Variables (Symbols, units)	Levels		
		Low (-)	Center (0)	High (+)
1	Current density; i (A m^{-2})	729	1000	1274
2	Catholyte load; L ($\text{kg m}^{-2} \text{ s}^{-1}$)	1.6	2.9	4.3
3	Pressure; P^a (kPa)	425	525	700
4	A336 conc.; S (mM)	0	0.66	1

^a Absolute outlet reactor pressure.

from $\Delta p_{\text{LG}} = 1.72 \times 10^5 \text{ Pa m}^{-1}$ (without A336) to $\Delta p_{\text{LG,A336}} = 3.45 \times 10^5 \text{ Pa m}^{-1}$ (with A336).

Furthermore, the pressure gradient associated with the movement of O_2 gas bubbles in liquid-filled capillaries with surfactant present $\Delta p_{\text{G},\gamma}^*$, has been estimated using the Herbolzheimer-Park model (for details, see Appendix B). It was found (Table IV) that the model calculation pressure gradient $\Delta p_{\text{G},\gamma}^*$ matched the gas-phase pressure gradient obtained from experimental data in the presence of A336, $\Delta p_{\text{G,A336}}$ (for calculation details see Appendix B). Therefore, it is plausible to assume that in the presence of A336 at high (*i.e.*, 475 kPa) operating pressure, surface tension gradients arise at the G/L interface, increasing the pressure gradient and furthermore, diminishing the surface excess concentration of A336 at the solid [*i.e.*, electrode-liquid (S/L)] interface. The latter effects are less significant at low pressure (*i.e.*, 200 kPa) where only a 20-30% increase of two-phase pressure gradient has been observed in the presence of A336. These considerations could explain the negative two-factor interaction between surfactant and pressure with respect to both H_2O_2 concentrations and current efficiency, Eq. 3 and 4, respectively.

A decrease of A336 S/L surface excess with increasing pressure is supported by a surfactant mass balance that accounts for the equilibrium distribution of A336 between the G/L and S/L interfaces and depends on the A336 feed concentration, the respective adsorption isotherms, the gas bubble diameter, the liquid hold-up, and the specific surface area of the electrodes. The A336 surface excess concentration at complete monolayer coverage is $3.25 \times 10^{-6} \text{ mol m}^{-2}$.¹⁰ Assuming no micelles, Langmuir adsorption, monolayer at the G/L, and bilayer at the S/L interface,¹⁰ and a liquid hold-up of 50%, the ideal gas law predicts an increase of the specific surface area from 2.0×10^5 to $2.7 \times 10^5 \text{ m}^2 \text{ m}^{-3}$ as the pressure is raised from 200 to 475 kPa and the bubble diameter decreases from 13.5 to 10 μm , resulting in a 2% decrease in the S/L surface excess of A336. This change in A336 S/L surface excess is sensitive to the liquid hold-up such that if the liquid hold-up drops to 30% the predicted S/L surface excess drops by about 37% compared to its value at 50% liquid hold-up at 200 kPa. Since it is known that liquid hold-up in trickle beds is smaller for foaming vs. nonfoaming liquids (*i.e.*, due to an increase of the Weber number),³⁰ there is a good possibility that the combined effect of pressure and A336 on the peroxide efficiency is caused by the corresponding redistribution of the surfactant between the G/L and S/L surfaces, as outlined above.

Factorial experimental design: acid electrolyte pH 3.—Employing the GF cathode a factorial experimental design of O_2 electroreduction to H_2O_2 in 1 M Na_2SO_4 (pH 3 acidified by glacial acetic acid) was carried out, using four variables at two levels and a centerpoint (*i.e.*, $2^4 + 1$ design). The variables and their levels are given in Table V. According to the $2^4 + 1$ experimental design created with the Jass 2.1 software seventeen experiments were per-

Table VI. Design matrix and responses (in random order) for the factorial runs in 1 M Na_2SO_4 (pH 3).

No.	Variable levels				H_2O_2 concentration (mM) ^a	Current efficiency (%) ^b	Reactor voltage (V) ^c
	i	L	P	S			
1	0	0	0	0	30 ± 1	53 ± 2	7.55 ± 0.18
2	-	+	+	+	22	80	6.05
3	-	+	-	+	17	60	6.60
4	+	+	-	+	20	40	8.70
5	+	-	-	+	46	35	8.75
6	+	+	-	-	15	31	10.60
7	-	+	+	-	16 ± 1	58 ± 4	6.05
8	-	-	-	-	28	38	6.40
9	-	-	+	-	34 ± 0.6	46 ± 1.7	6.50
10	+	+	+	-	23	49	8.20
11	-	-	-	+	37	49	6.70
12	+	-	+	-	36	28	8.40
13	+	+	+	+	30	62	7.97 ± 0.17
14	-	+	-	-	12	44	5.20
15	+	-	+	+	45 ± 1	35 ± 1	8.50 ± 0.10
16	-	-	+	+	43	57	6.50
17	+	-	-	-	32	25	8.45

^a Average factorial response: 29 mM. Pooled standard deviation: ± 0.8 mM.

^b Average factorial response: 46.5%. Pooled standard deviation: $\pm 1.8\%$.

^c Average factorial response: 7.47 V. Pooled standard deviation: ± 0.15 V.

formed. The experiments and the results obtained are summarized in Table VI. The outlet pH of the electrolyte varied between 3.8 and 5.0.

Under the employed conditions the highest H_2O_2 concentration per pass was about 45 mM obtained at low liquid load combined with high superficial current density (runs no. 5 and 15, Table VI). The highest current efficiency on the other hand, *i.e.*, 80% (run no. 2), has been obtained under opposite conditions, of low current density and high liquid load.

Neglecting the statistically insignificant effects, the three figures of merit in the case of the acidic media are described by the following regression model

$$C_{\text{H}_2\text{O}_2} \text{ (mM)} = 29 + 2.35X_I - 9.15X_L + 2.6X_P + 4X_S + 0.75X_LX_P - 1.15X_LX_S + 1.15X_PX_LX_P \quad [6]$$

$$CE(\%) = 46.5 + 6.9X_L - 7.95X_I + 5.7X_P + 6.3X_S + 3.45X_LX_P \quad [7]$$

$$E_{\text{reactor}}(\text{V}) = 7.47 + 1.23X_I - 0.21X_P + 0.23X_PX_L - 0.23X_PX_S - 0.22X_PX_S - 0.23X_PX_LX_S \quad [8]$$

where the coded variables are given by

$$X_I = \frac{i - 1001.5}{272.5}, \quad X_P = \frac{P - 562.5}{137.5},$$

$$X_S = \frac{S - 0.5}{0.5}, \quad \text{and} \quad X_L = \frac{L - 2.95}{1.35}$$

As shown by Eq. 6-8, the average values of the three figures of merit were: H_2O_2 concentration 29 ± 0.8 mM, current efficiency for H_2O_2 $46.5 \pm 1.8\%$, and reactor voltage 7.47 ± 0.15 V. These values indicate a poorer overall reactor performance as compared to the alkaline electrolyte (section on Alkaline electrolyte pH 9.6; factorial experiments).

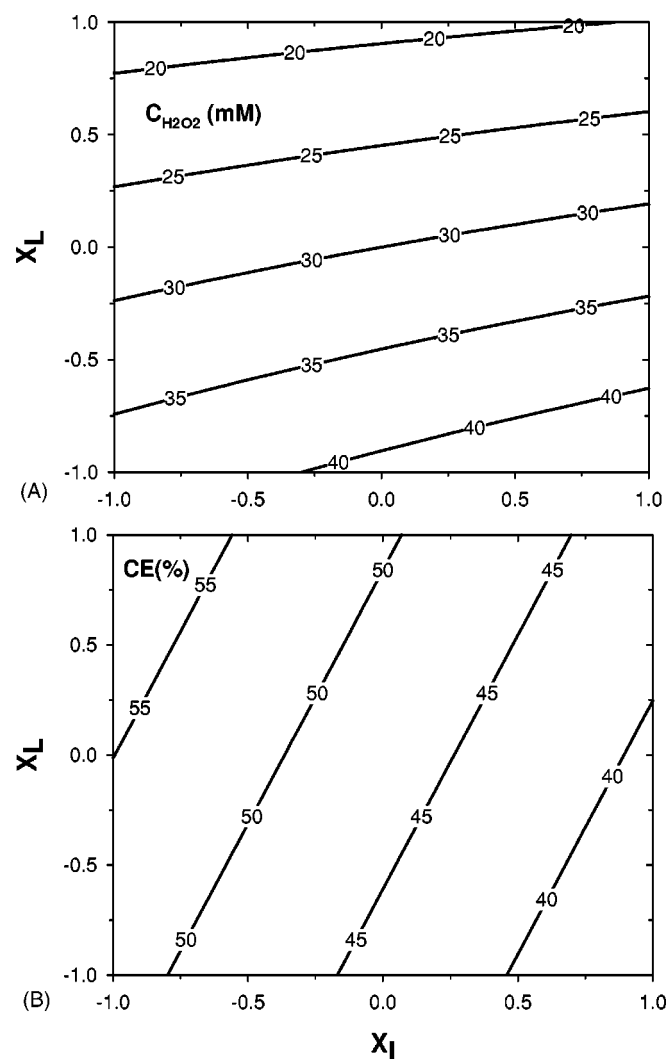


Figure 9. Contour plot of the factorial regression model for electroreduction of O_2 in 1 M Na_2SO_4 (pH 3 acidified with glacial acetic acid) on GF. $X_S = 1$ and $X_P = -1$. (A) H_2O_2 concentration, (B) current efficiency.

The cationic surfactant had a significant positive main effect on both H_2O_2 concentration and current efficiency, as indicated by Eq. 6 and 7, respectively. Similarly to the alkaline media, the main effect of A336 was larger than the one due to pressure. However, the pressures main effect was higher in acidic than in alkali conditions (compare Eq. 7 and 4). The main effect of A336 is very well illustrated by a comparison between runs no. 2 and 7 in Table VI. At $729 A m^{-2}$ the current efficiency was 58% without A336, while the corresponding current efficiency with A336 was 80%.

The two-factor pressure-surfactant interaction effect was overall statistically insignificant in acidic solution, suggesting that interfacial mechanisms similar to the one described for the alkaline electrolyte case, might be operative in offsetting the beneficial effect of high pressure in the presence of surfactant (e.g., compare runs no. 5 and 15, Table VI).

Equation 6 and 7 have been plotted as contour plots as a function of both X_1 and X_L for $X_S = 1$ and $X_P = -1$ (Fig. 9). To obtain current efficiencies $>50\%$, the liquid load and superficial current density must satisfy the following condition: $X_L \geq 0$ and $X_1 \leq -0.6$. The expected H_2O_2 concentration, on the other hand, would be less than 30 mM (Fig. 9).

Conclusions

The effect of four process variables, superficial current density, liquid load, pressure, and cationic surfactant concentration (i.e., trioctylmethylammonium chloride, A336) on the O_2 electroreduction to H_2O_2 was investigated using three-dimensional fixed-bed cathodes of GF and RVC.

The cathode was operated with co-current upward gas-liquid flow in either surging or pulsing regimes. The O_2 pressure was between 200 and 700 kPa(abs) (abs, absolute pressure). Two different electrolyte compositions were employed, with pH of 9.6 and 3, respectively. The higher O_2 mass-transfer capacity of GF compared to RVC under all the conditions explored here, allows the GF to operate with current efficiency above 70% (with A336) up to about $700 A m^{-2}$ (pH 3) and $2,700 A m^{-2}$ (pH 9.6) while with the same efficiency RVC operates only up to about $470 A m^{-2}$ (pH 3) and $680 A m^{-2}$ (pH 9.6).

A complete factorial experimental design with four variables at two levels and one centerpoint, revealed a positive main effect for A336 in both alkaline and acidic electrolytes with regard to current efficiency and peroxide concentration. The surfactant effect was attributed to lowering the rate of both H_2O_2 electroreduction and surface-catalyzed non-faradaic H_2O_2 decomposition. Using RVC operated at $300 A m^{-2}$, it was found that in acidic conditions, electroreduction is the major route of peroxide loss, while in alkaline conditions both the faradaic and non-faradaic peroxide losses must be taken into account. Future studies should also look at the impact of carbon surface chemistry on both the H_2O_2 electroreduction and surface-catalyzed decomposition.

Additionally, the enhancement of the $2e^- O_2$ reduction rate induced by A336 surface film formation, as previously proposed by the present authors, should be taken into account.¹⁰ The surfactant effect on O_2 reduction is probably more relevant in the acidic electrolyte where the O_2 electroreduction kinetics is sluggish.

In the 0.5 M Na_2CO_3 -0.5 M $NaHCO_3$ mixture (pH 9.6), a H_2O_2 concentration per single pass of 400 mM was obtained with a current efficiency of 84%, at $4650 A m^{-2}$ with 3 mM A336 in the electrolyte, 200 kPa pressure, $1.7 kg m^{-2} s^{-1}$ liquid, and $0.27 kg m^{-2} s^{-1} O_2$ load, respectively. Under identical conditions but without A336, the current efficiency was 63%, corresponding to an H_2O_2 concentration of 300 mM.

Furthermore, in alkali a negative interaction effect was found between the A336 concentration and operating pressure. The Herbolzheimer-Park model of the gas-phase pressure gradient due to surface tension differences acting along the length of gas bubbles gave a good agreement with the experimentally measured data. The measured two-phase flow pressure gradient in the fiber bed increased in the presence of cationic surfactant by up to 100%. It is proposed that the negative interaction effect between surfactant and operating pressure is due to diminished A336 surface excess concentration at the solid(electrode)-liquid interface, as a result of surfactant mass transfer to the gas-liquid interface to counteract the surface tension gradients created at high operating pressure.

The long-term stability of the figures of merit is an important aspect for the scale-up of the O_2 electroreduction process. All experiments in the factorial design were completed with the same electrodes and this amounted to a total of about 50 h of reactor operation. During this time the reproducibility of the experiments was satisfactory, as indicated in the statistically designed experimental analysis. Furthermore, collateral in-house data showed that during continuous operation of a similar peroxide electrosynthesis reactor using a graphite felt cathode and commercial grade NaOH over a 30 day period the current efficiency fell by about 0.3% per day. The drop in current efficiency was due to decomposition of peroxide by the accumulated transition metal ions from the feed liquid. In that collateral work the current efficiency was restored by washing the reactor with dilute HNO_3 or alternatively the drop in current efficiency was suppressed by the presence of chelating agents in the feed solution.⁴⁵

Future work should look at optimizing the process variables in conjunction with scale-up of the three-dimensional electrodes with various configurations (*e.g.*, bipolar stack). Moreover, in addition to A336, other cationic surfactants could be evaluated for potentially improved performance especially in acidic conditions.

Acknowledgments

The authors gratefully acknowledge financial support from the Network of Centers of Excellence (Mechanical Wood Pulps) of the Government of Canada and the Natural Sciences and Engineering Research Council of Canada, as well as from the University of British Columbia New Faculty Start-Up Fund (E.G.).

The University of British Columbia assisted in meeting the publication costs of this article.

Appendix A

Modeling of O_2 reduction to H_2O_2 in GF and RVC electrodes under mass-transfer limiting conditions: The effect of cationic surfactant A336.—For both three-dimensional electrodes (*i.e.*, GF and RVC) the mass-transfer limiting superficial current density for O_2 reduction i_{ml,O_2} ($A\ m^{-2}$), is expressed as

$$i_{ml,O_2} = nFK_{mc,O_2}\tau_1 C_{O_2} \quad [A-1]$$

where C_{O_2} is the O_2 concentration in the electrolyte ($mol\ m^{-3}$), F is the faraday constant, ($C\ mol^{-1}$), K_{mc,O_2} is the overall O_2 mass-transfer capacity (s^{-1}), n , the no. of electrons transferred ($=2$), and τ_1 is the maximum electroactive bed thickness in the direction of current flow operating at the limiting current density (m).

The O_2 concentration in the employed electrolyte solutions (*i.e.*, either a mixture of 0.5 M Na_2CO_3 -0.5 M $NaHCO_3$ or 1 M Na_2SO_4) can be estimated from a modified Sechenov equation^{35,36}

$$\log\left(\frac{C_{O_2,0}}{C_{O_2}}\right) = \sum_j k_{s,j}C_{salt,j} \quad [A-2]$$

where $C_{O_2,0}$ is the O_2 concentration in pure water at a given pressure and temperature,³⁷ $C_{salt,j}$ is the concentration of salt j , ($mol\ m^{-3}$) and $k_{s,j}$ is the Sechenov constant for salt j ($m^3\ mol^{-1}$), given by

$$k_{s,j} = \sum_i (h_i + h_{O_2})z_i \quad [A-3]$$

with h_{O_2} gas-specific parameter (for O_2 is equal to zero³⁵), h_i ion-specific parameter for salt j ($m^3\ mol^{-1}$) (*i.e.*, for Na^+ : 1.079×10^{-4} , SO_4^{2-} : 1.164×10^{-4} , CO_3^{2-} : 1.158×10^{-4} , and HCO_3^- : 1.019×10^{-4} ³⁵), and z_i is the number of ions i in the composition of salt j .

Furthermore, the presence of A336 increases the solubility of O_2 in the electrolytes under consideration by a factor of about 1.1.¹⁰

The expression of the maximum electroactive thickness in Eq. A-1 τ_1 is dependent on the relationship between the effective specific conductivity of the electrolyte $\kappa_{L,eff}$ and the effective electronic conductivity of the solid matrix (GF or RVC) σ (see Table I).³⁸ Thus

$$\text{for } \kappa_{L,eff} < \sigma; \quad \tau_1 = \left(\frac{2\kappa_{L,eff}\Delta\Phi_{max,1}}{nFK_{mc,O_2}C_{O_2}}\right)^{1/2} \quad [A-4]$$

while

$$\text{for } \kappa_{L,eff} \equiv \sigma; \quad \tau_1 = \left(\frac{4\kappa_{L,eff}\Delta\Phi_{max,1}}{nFK_{mc,O_2}C_{O_2}}\right)^{1/2} \quad [A-5]$$

In Eq. A-4 and A-5 $\kappa_{L,eff}$ can be estimated by³⁹

$$\kappa_{L,eff} = \frac{2\kappa_L\varepsilon_{eff}}{3 - \varepsilon_{eff}} \quad [A-6]$$

where ε_{eff} is the effective porosity of the bed with respect to the liquid phase (Eq. A-7 and A-8), while the specific ionic conductivities κ_L of the electrolytes under study have been experimentally measured. For both electrolyte compositions (*i.e.*, alkaline and acidic) κ_L was $8\ S\ m^{-1}$. Therefore, the assumption of $\kappa_{L,eff} < \sigma$ has been made (see also Table I) and Eq. A-4 has been used to estimate τ_1

$$\varepsilon_{eff} = \beta_L \cdot \varepsilon \quad [A-7]$$

where β_L is liquid hold-up and ε is the porosity of the three-dimensional matrix (Table I).

The liquid hold-up β_L in the graphite fiber bed is given by the Hodgson-Oloman correlation³⁴

$$\beta_L = 1 - 0.907L^{-0.362}G^{0.301}, \quad 0 < G < 0.35\ kg\ m^{-2}\ s^{-1}, \\ \text{and } 1.53 < L < 7.62\ kg\ m^{-2}\ s^{-1} \quad [A-8]$$

where L and G are the liquid and gas load, respectively ($kg\ m^{-2}\ s^{-1}$).

In Eq. A-4 the maximum tolerable (theoretical) electrode potential difference $\Delta\Phi_{max,1}$ across the bed thickness with negligible secondary reaction (*i.e.*, H_2O_2 electroreduction) was evaluated as the width of the O_2 reduction limiting current plateau.³⁸ Employing polarization curves published in the literature $\Delta\Phi_{max,1}$ was assumed equal to 0.1 V in alkaline^{10,11,28} and 0.03 V in the acidic electrolyte,^{10,19} respectively.

The presence of the cationic surfactant A336 had a profound influence on the O_2 polarization behavior, shifting the O_2 reduction wave and peak potential to positive values. At the A336 concentration of the present work the magnitude of the peak potential shift was about 0.3 V in carbonate and about 0.09 V in acid.¹⁰ Therefore, it was assumed that in the presence of the cationic surfactant, $\Delta\Phi_{max,1}$ is about 0.3 V in the alkaline and 0.09 V in the acidic electrolyte.

The overall O_2 mass-transfer capacity K_{mc,O_2} for two-phase co-current upward flow in GF could be estimated using the correlation presented by Hodgson and Oloman³⁴

$$K_{mc,O_2,GF} = 5.9L^{0.372}G^{0.232} \quad [A-9]$$

For reticulated vitreous carbon electrodes on the other hand, there has been no comprehensive study of the two-phase gas-liquid mass transfer.

Therefore, the two-phase O_2 mass-transfer coefficient in RVC was estimated as the contribution of three mechanisms, *i.e.*, single liquid-phase convective flow mass transfer in the RVC K_0 , boundary-layer disturbance effect due to gas bubbles induced local turbulence K_d , and penetration mechanism where the gas bubbles have the role of injecting O_2 very near to the electrode surface, (*i.e.*, virtually gas-solid mass transfer) K_p .

The mass-transfer coefficient due to boundary-layer disturbance mechanism K_d in the RVC electrode could be assessed using the correlation reported by Sedahmed *et al.* for inert gas-sparged fixed-bed electrodes composed of vertical screen stacks⁴⁰

$$St = 0.2(Re_G Fr_G)^{-0.26} Sc^{-0.66} \left(\frac{\tau_m}{d}\right)^{-0.28} \quad [A-10]$$

where

$$St = \frac{K_d}{u_G}, \quad Re_G = \frac{u_G d}{\nu_L}, \quad Sc = \frac{\nu_L}{D_{O_2}}, \quad \text{and } Fr_G = \frac{u_G^2}{d \cdot g} \quad [A-11]$$

with d the vitreous carbon filament diameter (5.3×10^{-5} m for RVC 39 ppc, Table I), D_{O_2} diffusion coefficient of O_2 in the electrolyte solution (*i.e.*, 5×10^{-10} $m^2\ s^{-1}$ at 298 K²), g acceleration due to gravity ($m^2\ s^{-1}$), u_G superficial gas velocity ($m\ s^{-1}$), ν_L kinematic electrolyte viscosity ($m^2\ s^{-1}$), and τ_m geometric thickness of the RVC electrode (m).

The liquid-phase convective mass-transfer coefficient in RVC K_0 is given by the Fenton-Alkire correlation⁴¹

$$Sh = 11Re_L^{0.3} \quad [A-12]$$

where

$$Sh = \frac{K_0\varepsilon_{eff}}{a_{LS}D_{O_2}} \quad \text{and } Re_L = \frac{u_L}{a_{LS}\varepsilon_{eff}\nu_L} \quad [A-13]$$

with a_{LS} the specific surface area available for liquid-solid mass transfer ($m^2\ m^{-3}$) and u_L , the superficial liquid velocity ($m\ s^{-1}$).

Last, the penetration mechanism mass-transfer coefficient K_p was obtained by extrapolating the data reported by Takahashi and Alkire⁴² to the Re_L and Re_G values employed in the present work. It was found that

$$K_p \equiv 2K_d \quad [A-14]$$

The overall O_2 mass-transfer capacity in RVC $K_{mc,O_2,RVC}$ was expressed as

$$K_{mc,O_2,RVC} = a_{LS}(K_0 + K_d) + a_{GS}K_p \quad [A-15]$$

with

$$a_{LS} = \beta_L a_m \quad \text{and } a_{GS} = (1 - \beta_L) a_m \quad [A-16]$$

where a_{GS} , a_{LS} , are the specific surface area available to gas-solid and liquid-solid mass transfer, respectively, while a_m is the specific surface area of the RVC matrix (Table I) and β_L was estimated by Eq. A-8.

Table A-I. Mass-transfer capacity, maximum electroactive bed thickness and superficial limiting current density for O₂ reduction on GF and RVC electrodes. Conditions corresponding to Fig. 5 and 6 (pH 9.6) and Fig. 7 (pH 3), respectively.

3D electrode	Electrolyte	K_{mc,O_2} (s ⁻¹)	$\Delta\Phi_{max,1}^a$ (V)	τ_1 (m)	i_{m1,O_2} (A m ⁻²)
GF	Mixture of: 0.5 M Na ₂ CO ₃ 0.5 M NaHCO ₃ (pH 9.6) 1 M Na ₂ SO ₄ (acidified to pH 3)	6.7	0.1 (A336 = 0)	6.0×10^{-4}	1520
			0.3 (A336 = 3 mM)	9.0×10^{-4}	2760
			0.03 (A336 = 0)	3.0×10^{-4}	1040
			0.09 (A336 = 1 mM)	4.0×10^{-4}	1890
			0.1 (A336 = 0)	2.5×10^{-3}	370
RVC	Mixture of: 0.5 M Na ₂ CO ₃ 0.5 M NaHCO ₃ (pH 9.6) 1 M Na ₂ SO ₄ (acidified to pH 3)	0.38	0.3 (A336 = 1 mM)	4.1×10^{-3}	680
			0.03 (A336 = 0)	1.1×10^{-3}	260
			0.09 (A336 = 1 mM)	1.8×10^{-3}	470

^a Reflects the estimated effect of the cationic surfactant (A336) on the polarization curves for O₂ and H₂O₂ reduction. The presence of A336 increases $\Delta\Phi_{max,1}$.

Equations A-2 to A-16, have been applied to calculate the O₂ mass-transfer limiting superficial current density i_{m1,O_2} expressed by Eq. A-1. Table A-I summarizes the mass-transfer capacity, maximum electroactive thickness, and limiting current density for the experimental conditions relevant to Fig. 5-7.

Appendix B

Effect of surfactant on the gas-phase pressure gradient in the graphite fiber bed.—The pressure gradient required to drive a gas bubble through a liquid-filled capillary in the presence of surfactant can be estimated using the Herbolzheimer-Park model^{3f}

$$\Delta p_{G,\gamma}^* = \frac{\Delta P_{G,\gamma}^*}{H_c} = 0.942\gamma Ca^{1/3} \frac{l_b}{H_c \cdot r_b^2} \quad [B-1]$$

where $\Delta P_{G,\gamma}^*$ and $\Delta p_{G,\gamma}^*$ are the pressure drop (Pa) and pressure gradient (Pa m⁻¹), respectively, associated with the movement of the bubble in the liquid-filled capillary with surfactant present, H_c is the effective height of the 3D cathode (m) (Fig. 1), l_b and r_b are the length and menisci radius of the bubble, respectively (m), γ is surface tension (N m⁻¹), and Ca is the dimensionless capillary number defined as

$$Ca = \frac{\mu_L u_{b,eff}}{\gamma} \quad [B-2]$$

with $u_{b,eff}$ effective gas bubble velocity in the capillary filled with liquid (m s⁻¹) and μ_L the liquid dynamic viscosity (Pa s). The effective gas bubble velocity in the liquid-filled portion of the bed can be estimated as

$$u_{b,eff} = \frac{u_G}{\varepsilon\beta_L} \quad [B-3]$$

where u_G is the superficial gas velocity (m s⁻¹), β_L is liquid hold-up (Eq. A-8) and ε is the porosity of the 3D matrix (Table I).

In Eq. B-1 and B-2 it was assumed that $\gamma = 30 \times 10^{-3}$ N m⁻¹ in the presence of 3 mM A336, and a typical O₂ gas bubble dimension in the graphite felt electrode (Fig. 2A) was considered to be $l_b = 8 \times 10^{-5}$ m and $r_b = 5 \times 10^{-6}$ m, respectively.

In the absence of surfactant the pressure gradient associated with the movement of a bubble in a capillary filled with liquid is expressed by the Bretherton equation (for a review, see Ref. 31).

$$\Delta p_G^* = \frac{\Delta P_G^*}{H_c} = 9.4Ca_0^{2/3} \frac{\gamma_0}{H_c \cdot r_b} \quad [B-4]$$

where γ_0 is the surfactant-free surface tension of the electrolyte ($\sim 70 \times 10^{-3}$ N m⁻¹), Ca_0 is the capillary number corresponding to the surfactant-free case.

Using the experimentally measured two-phase pressure gradient data Δp_{LG} and $\Delta p_{LG,A336}$ (i.e., in the absence and presence of A33), the gas-phase pressure gradients $\Delta p_{G,A336}$ and Δp_G with and without surfactant present were calculated and compared to the gas-phase pressure gradients obtained from the Herbolzheimer-Park Eq. B-1 $\Delta p_{G,\gamma}^*$ and Bretherton equation, B-4 Δp_G^* , respectively (Table IV).

To estimate $\Delta p_{G,A336}$ and Δp_G from the experimentally measured two-phase data, the following approach has been adopted. For graphite fiber beds similar to the one used here, Hodgson and Oloman have shown that the two-phase pressure gradient is best described by the Sato correlation where the respective single-phase values are expressed by the Ingmanson equation (for a critical review of various correlations and applicability to fiber-beds see Ref. 34).

$$\log \left[\frac{\Delta p_{LG}}{\Delta p_L(1 + 1/Y^2)} \right] = \frac{0.7}{[\log(Y/1.2)]^2 + 1} \quad [B-5]$$

where $Y = (\Delta p_L/\Delta p_G)^{1/2}$ is the Lockart-Martinelli parameter, whilst Δp_{LG} , Δp_G , and Δp_L are the pressure gradients (Pa m⁻¹) for the two-phase, gas and liquid single-phases, respectively.

The liquid-phase pressure gradient in fiber beds is³⁴

$$\Delta p_L = 10^{-11} \frac{k(1 - \varepsilon^2)}{\varepsilon^3} \mu_L \cdot u_L \cdot a_f^2 \quad [B-6]$$

where a_f is the specific area of the fiber [$=4/d_f$, d_f fiber diameter (m)], k is the Kozeny constant for fibrous beds given by Eq. B-7, and u_L is the liquid superficial velocity (m s⁻¹)

$$k = 3.6 \frac{\varepsilon^3}{(1 - \varepsilon)^{1/2}} [1 + 57(1 - \varepsilon)^3] \quad [B-7]$$

Using the experimentally measured Δp_{LG} and $\Delta p_{LG,A336}$ together with Δp_L calculated from Eq. B-6-B-7, the gas-phase pressure gradients for the two scenarios, $\Delta p_{G,A336}$ and Δp_G , were obtained from Eq. B-5.

Table IV summarizes both the experimentally determined and calculated pressure gradients, Δp_{LG} , $\Delta p_{LG,A336}$, Δp_G , $\Delta p_{G,A336}$ together with the gas-phase pressure gradients obtained from the Herbolzheimer-Park and Bretherton models $\Delta p_{G,\gamma}^*$ and Δp_G^* for the cases with and without surfactant present, respectively.

List of Symbols

a	specific surface area (m ² m ⁻³)
d	fiber diameter (m)
C	concentration (mol m ⁻³ or mM)
Ca	capillary number
D	diffusion coefficient (m ² s ⁻¹)
E^0	standard electrode potential (V vs. SHE)
$E_{reactor}$	reactor voltage (V)
F	Faraday's constant (=96,485.3 C mol ⁻¹)
Fr	Froude number
g	gravitational acceleration (m ² s ⁻¹)
G	gas load (kg m ⁻² s ⁻¹)
i	superficial current density (A m ⁻²)
h	ion and gas specific parameter in the modified Sechenov equation (m ³ mol ⁻¹)
H_c	height of the 3D cathode (m)
k	Kozeny constant (dimensionless)

- k_s Sechenov constant ($\text{m}^3 \text{mol}^{-1}$)
 K O_2 mass-transfer coefficient (m s^{-1})
 K_{mc} O_2 mass transfer capacity (s^{-1})
 l length (m)
 L liquid load ($\text{kg m}^{-2} \text{s}^{-1}$)
 n total nr. of electrons exchanged in the primary reaction (=2)
 Δp pressure gradient (i.e. pressure drop per cathode length) (Pa m^{-1})
 P pressure (Pa or kPa absolute)
 ΔP pressure drop (Pa)
 r radius (m)
 Re Reynolds number
 S cationic surfactant (A336) concentration (mM)
 Sc Schmidt number
 Sh Sherwood number
 St Stanton number
 u fluid superficial velocity (m s^{-1})
 X coded variable in the factorial design (dimensionless) [$X = [y - (y_{\text{low}} + y_{\text{high}}/2)] / [(y_{\text{high}} - y_{\text{low}})/2]$, where y_{low} is the variable in the factorial design]
 Y Lockart-Martinelli parameter (dimensionless)
 z_j no. of ions i in the composition of the electrolyte
- Greek
- β_L liquid hold-up (dimensionless)
 ϵ porosity of the 3D electrode matrix (dimensionless)
 γ surface tension (N m^{-1})
 $\Delta\Phi_{\text{max},1}$ maximum tolerable potential drop without significant side reaction (V)
 κ specific ionic conductivity (S m^{-1})
 μ dynamic viscosity (Pa s)
 ν kinematic viscosity ($\text{m}^2 \text{s}^{-1}$)
 σ electronic conductivity (S m^{-1})
 τ thickness of the 3D electrode (m)
- Subscripts
- 0 single-phase convection or pure phase
 1 related to the primary reaction of $2e^- \text{O}_2$ reduction
 A336 in the presence of cationic surfactant A336
 b gas bubble
 d disturbance mechanism
 eff effective
 f fiber
 G gas phase
 L liquid phase
 m 3D electrode matrix
 ml mass-transfer limited
 O2 oxygen index
 p penetration mechanism
 S solid phase (i.e., electrode surface)
 wt indicates weight percentage
 γ related to surface tension difference
- Superscript
- * given by a model for gas bubble movement in a liquid-filled capillary
- Abbreviations
- abs absolute pressure
 CMC critical micelle concentration
 GF graphite felt
 RVC reticulated vitreous carbon
- References
1. J. Whiteside, *Pulp Pap. Int.*, **10**, 48 (1998).
 2. K. Kinoshita, *Electrochemical Oxygen Technology*, pp. 369, 8, John Wiley & Sons, Inc., New York (1992).
 3. C. Oloman, *Electrochemical Processing for the Pulp and Paper Industry*, p. 143, The Electrochemical Consultancy, Romsey, U.K. (1996).
 4. M. Nozaki, *Kami Pa Gikyoshi*, **52**, 616 (1998).
 5. J. R. Anderson and B. Amini, in *Pulp Bleaching: Principles and Practice*, C. W. Dence and D. W. Reeve, Editors, p. 413, Tappi Press, Atlanta, GA (1998).
 6. A. W. Rudie, T. J. McDonough, F. Rauh, R. J. Klein, J. L. Parker, and S. A. Heimburger, *J. Pulp Paper Sci.*, **19**, J47 (1993).
 7. G. X. Pan, S. Vichnevsky, and G. J. Leary, in *1998 Pulping Conference, Tappi Proceedings*, 637 (1998).
 8. T. Koshitsuka, *Kami Pa Gikyoshi*, **52**, 623 (1998).
 9. A. Paren and T. Tsujino, *Kami Pa Gikyoshi*, **52**, 630 (1998).
 10. E. L. Gyenge and C. W. Oloman, *J. Appl. Electrochem.*, **31**, 233 (2001).
 11. K. Vetter, *Electrochemical Kinetics: Theoretical and Experimental Aspects*, pp. 632, 639-641, Academic Press, New York (1967); (b) D. T. Sawyer, *Oxygen Chemistry*, p. 21, Oxford University Press, New York (1991).
 12. M. S. Wrighton, *Science*, **231**, 32 (1986).
 13. C. Degrand, *J. Electroanal. Chem.*, **169**, 259 (1984).
 14. O. El Mouahid, C. Coutanceau, E. M. Belgsir, P. Crouigneau, J. M. Leger, and C. Lamy, *J. Electroanal. Chem.*, **426**, 117 (1997).
 15. R. G. Compton, F. Marken, C. H. Goeting, R. A. J. McKeown, J. S. Foord, G. Scarsbrook, R. S. Sussmann, and A. J. Whitehead, *Chem. Commun. (Cambridge)*, **1998**, 1961.
 16. E. L. Gyenge and C. W. Oloman, *J. Appl. Electrochem.*, **33**, 655 (2003).
 17. E. L. Gyenge and C. W. Oloman, *J. Appl. Electrochem.*, **33**, 665 (2003).
 18. Y. Qingfeng, L. Xiaoping, and Z. Xiuling, *J. Appl. Electrochem.*, **33**, 273 (2003).
 19. J. S. Do and C. P. Chen, *J. Electrochem. Soc.*, **140**, 1632 (1993).
 20. C. Ponce de Leon and D. Pletcher, *J. Appl. Electrochem.*, **25**, 307 (1995).
 21. A. Alvarez-Gallegos and D. Pletcher, *Electrochim. Acta*, **44**, 853 (1998).
 22. A. Alvarez-Gallegos and D. Pletcher, *Electrochim. Acta*, **44**, 2483 (1999).
 23. W. Wagner and C. J. Hull, *Inorganic Titrimetric Analysis*, p. 130, Marcel Dekker, New York (1971).
 24. (a) B. N. Afanas'ev, Yu. P. Akulova, and L. V. Bykova, *Russ. J. Electrochem.*, **28**, 1524 (1992); (b) B. N. Afanas'ev, Yu. P. Skobochkina, and L. V. Bykova, *Russ. J. Electrochem.*, **27**, 454 (1991); English translation.
 25. (a) Z. M. Galbács and L. Csányi, *J. Chem. Soc. Dalton Trans.*, **79**, 417 (1983); (b) O. Špalek, J. Balej, and I. Paseka, *J. Chem. Soc., Faraday Trans.*, **78**, 2349 (1982); (c) H. B. Lee, A. H. Park, and C. Oloman, *Tappi J.*, **83**, 94 (2000); (d) J. A. Navarro, M. A. De La Rosa, M. Roncel, and F. F. De La Rosa, *J. Chem. Soc., Faraday Trans.*, **80**, 249 (1984).
 26. G. A. Kolyagin and V. L. Kornienko, *Russ. J. Appl. Chem.*, **76**, 1070 (2003); English translation.
 27. A. Storck, M. A. Latifi, G. Barhole, A. Laurent, and J. C. Charpentier, *J. Appl. Electrochem.*, **16**, 947 (1986).
 28. J. B. Davison, J. M. Kacsir, P. J. Pearce-Landers, and R. Jasinski, *J. Electrochem. Soc.*, **130**, 1497 (1983).
 29. D. C. Montgomery, *Design and Analysis of Experiments*, 4th ed., p. 228, John Wiley & Sons Inc., New York (1997).
 30. A. Gianetto and V. Specchia, *Chem. Eng. Sci.*, **47**, 3197 (1992).
 31. (a) R. F. Probst, *Physicochemical Hydrodynamics*, pp. 300-314, Butterworths Publishers, Boston (1989); (b) C. W. Park, *Phys. Fluids A*, **4**(11), 2335 (1992).
 32. D. J. Shaw, *Introduction to Colloid and Surface Chemistry*, 4th ed., p. 274, Butterworth-Heinemann Ltd., Oxford (1992).
 33. A. Mohandes, Ph.D. Thesis, The University of British Columbia, Vancouver, Canada (1994).
 34. I. Hodgson and C. Oloman, *Chem. Eng. Sci.*, **54**, 5777 (1999).
 35. C. Hermann, I. Dewes, and A. Schumpe, *Chem. Eng. Sci.*, **50**, 1673 (1995).
 36. A. Schumpe, *Chem. Eng. Sci.*, **48**, 153 (1993).
 37. *Perry's Chemical Engineers Handbook*, 6th ed., D. W. Green and J. O. Maloney, Editors, pp. 3-103, McGraw-Hill, Inc., New York (1984).
 38. A. I. Masliy and N. P. Podubnyy, *J. Appl. Electrochem.*, **27**, 1036 (1997).
 39. C. Oloman, *J. Electrochem. Soc.*, **126**, 1885 (1979).
 40. G. H. Sedahmed, H. A. Farag, A. A. Zatout, and F. A. Katkout, *J. Appl. Electrochem.*, **16**, 374 (1986).
 41. J. M. Fenton and R. C. Alkire, *J. Electrochem. Soc.*, **135**, 2200 (1988).
 42. K. Takahashi and R. Alkire, *Chem. Eng. Commun.*, **38**, 209 (1985).
 43. C. Oloman, Can. Pat. 1214747 (1986).